

# Saddle-point scrambling without thermalisation

R. A. Kidd,<sup>1,\*</sup> A. Safavi-Naini,<sup>2,1,3</sup> and J. F. Corney<sup>1</sup>

<sup>1</sup>*School of Mathematics and Physics, University of Queensland, Brisbane, Queensland 4072, Australia.*

<sup>2</sup>*ARC Centre of Excellence for Engineered Quantum Systems,*

*School of Mathematics and Physics, University of Queensland, Brisbane, QLD 4072, Australia*

<sup>3</sup>*Institute for Theoretical Physics, University of Amsterdam,  
Science Park 904, 1098 XH Amsterdam, the Netherlands*

(Dated: December 22, 2024)

Out-of-time-order correlators (OTOCs) have proven to be a useful tool for studying thermalisation in quantum systems. In particular, the exponential growth of OTOCs, or scrambling, is sometimes taken as an indicator of chaos in quantum systems, despite the fact that saddle points in integrable systems can also drive rapid growth in OTOCs. Here we use the simple model of the two-site Bose-Hubbard model to demonstrate how the OTOC growth driven by chaos can nonetheless be distinguished from that driven by saddle points. Besides quantitative differences in the long term average as predicted by the eigenstate thermalisation hypothesis, the saddle point gives rise to oscillatory behaviour not observed in the chaotic case. The differences are also highlighted by entanglement entropy, which in the chaotic Floquet case matches the Page curve prediction. These results illustrate additional markers that can be used to distinguish chaotic behaviour in quantum systems, beyond the initial exponential growth in OTOCs.

## I. INTRODUCTION

The dynamics of quantum information provides a link between different areas of physics, as is evident in the study of fast scrambling, quantified by the exponential growth of the out-of-time-order correlators (OTOCs) [1–6]. First introduced to describe the dynamics of quantum information in black holes, scrambling has since been used to probe the connections between the dynamics of entanglement, chaos, and thermalisation [7–12]. In particular, studies of chaotic models in periodically driven and undriven systems have used a variety of OTOC, including the fidelity out-of-time-order correlator (FOTOC), to show that, in the chaotic phase, the OTOC grows exponentially up to an Ehrenfest time, after which it saturates to a value predicted by the eigenstate thermalisation hypothesis (ETH) [7–11, 13–16]. According to the ETH, if the state of an isolated quantum system is sufficiently delocalised in the basis of energy eigenstates, the system will relax towards the ‘diagonal ensemble’ (DE) due to dephasing between energy eigenstates [17, 18]. Consequently, in the absence of an external drive an initial product state will evolve to a finite-temperature thermal state with volume-law entanglement entropy, whereas a periodically driven system will evolve to an infinite-temperature state [10, 13, 14, 16, 17].

More recently it has been shown that although chaos is a sufficient condition for the exponential growth of the OTOC, it is not a necessary one [12, 15, 19–24]. In fact, scrambling and the exponential growth of an OTOC may be driven by an unstable trajectory associated with a hyperbolic fixed point—or saddle point—in the semiclassical phase space. So far, scrambling

without chaos has been observed in Ising spin chains with long-range interactions [19], the truncated Lieb-Liniger model [20], the inverted harmonic oscillator [21–24], the Dicke model [15] and the Lipkin-Meshkov-Glick model [12]. Saddle-dominated scrambling in the presence of chaos has been observed in the kicked rotor model, the Feingold-Peres model of coupled tops and elastic manifolds pinned in a random potential [12].

In this paper we study the entanglement dynamics in the two-site Bose-Hubbard model, showing explicit differences between the chaotic and the saddle point regimes. This model, which could be experimentally implemented in ultracold atoms, allows access to stable, unstable (chaotic), and saddle-point regions in phase-space through tuning and modulation of the inter-well tunnelling rate. We solve exactly the short-time and long-time (times much longer than the Ehrenfest time) dynamics for up to  $10^3$  particles. In the chaotic regime, OTOCs grow exponentially until saturating at the ETH prediction, consistent with thermalisation. In contrast, we find that the saddle point FOTOC exhibits large, long-lived oscillations around the diagonal ensemble prediction. These differences can be traced back to distinct differences in the respective diagonal ensembles, reflected quantitatively in the Shannon entropy. We also study the long-time behaviour of the von Neumann entanglement entropy, and its scaling with subsystem size, to highlight the differences between the two regimes and confirm the lack of thermalisation at the saddle point.

## II. MODEL

In this work we consider the Bose-Hubbard dimer [25], which is described by the Hamiltonian,

$$\hat{H} = 2U\hat{S}_z^2 - 2J\hat{S}_x, \quad (1)$$

\* ryan.kidd@uq.edu.au

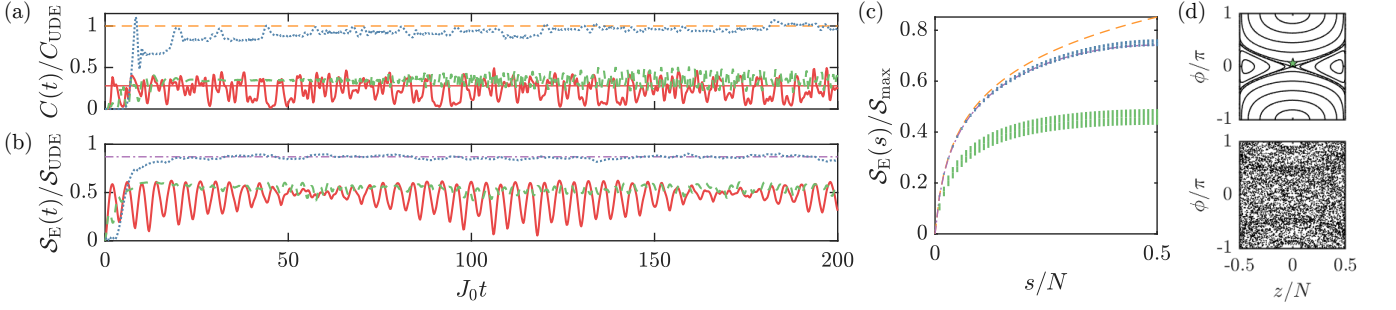


FIG. 1. a) Fidelity out-of-time-order correlators (FOTOCs) for chaotic phase space (blue dotted line), a saddle point (thick red line) and a point slightly perturbed from the saddle point (green dashed line) for  $N = 1000$  particles. The infinite-temperature uniform diagonal ensemble (UDE) prediction is indicated by the horizontal thin yellow dashed line. The saddle point state diagonal ensemble prediction is indicated by the horizontal thin red line. b) Von Neumann entanglement entropy for a subsystem of  $s = N/2$  Dicke states and  $N = 100$  particles. The Page curve prediction is indicated by the thin purple dash-dotted line. c) Post-Ehrenfest time-averaged von Neumann entanglement entropy for the chaotic (blue error bars) and saddle-perturbed (green error bars) states, with two standard deviations indicated by bar height. Entanglement entropy is averaged over  $20 \leq J_0 t \leq 200$ . d) Semiclassical phase space for the regimes with a saddle point (top:  $NU = -2$ ,  $J = 1$ ) and chaos (bottom:  $NU = -1$ ,  $J(t) = 1 + 1.5 \cos(0.5t)$ ). The perturbed state  $(z, \phi/\pi) = (0, 0.06)$  is indicated by the green star. The phase space representation is periodic in  $\phi \in [-\pi, \pi]$ .

where  $J$  is the tunneling strength and  $U$  is the on-site interaction energy. We use the pseudo-angular-momentum operators  $\hat{S}_\alpha$  with  $\alpha = x, y, z$ ,

$$\begin{aligned}\hat{S}_x &= \frac{\hat{a}_2^\dagger \hat{a}_1 + \hat{a}_1^\dagger \hat{a}_2}{2}, \\ \hat{S}_y &= \frac{\hat{a}_2^\dagger \hat{a}_1 - \hat{a}_1^\dagger \hat{a}_2}{2i}, \\ \hat{S}_z &= \frac{\hat{a}_2^\dagger \hat{a}_2 - \hat{a}_1^\dagger \hat{a}_1}{2},\end{aligned}\quad (2)$$

where  $\hat{a}_j$ ,  $\hat{a}_j^\dagger$  with  $j = 1, 2$  are the creation and annihilation operators for the two bosonic modes and  $[\hat{S}_\alpha, \hat{S}_\beta] = i\epsilon_{\alpha\beta\gamma}\hat{S}_\gamma$ .

The semiclassical phase space of the two-site Bose-Hubbard model is shown in Fig. 1(d) in two different regimes, using coordinates  $z = \langle \hat{S}_z \rangle$  and  $\phi = -\arg(\langle \hat{S}_x \rangle + i\langle \hat{S}_y \rangle)$ . For  $NU \leq J$ , the system undergoes Rabi oscillations and the phase space fixed points are two stable centres [25]. At the critical interaction strength,  $NU/J = 1$ , the  $z, \phi = 0$  stable centre undergoes a pitchfork bifurcation. For stronger interactions, ‘self-trapping trajectories’ emerge on either side of a hyperbolic fixed point [25], as shown in the upper plot in Fig. 1(d).

The addition of periodic modulation to the tunneling frequency,  $J(t) = J_0[1 + \mu \cos(\omega t)]$  makes the two-site Bose-Hubbard model chaotic [26], as shown in the lower plot in Fig. 1(d). The extent of the chaos can be finely controlled using the modulation constants  $\mu, \omega$  [16, 26, 27].

### III. RESULTS

To study the entanglement dynamics, we use the FOTOC given by  $C(t) \equiv \langle \hat{W}_\delta(t) \hat{V}(0) \hat{W}_\delta(t) \hat{V}(0) \rangle$ , where  $\hat{W}_\delta$  is an arbitrary rotation with generator  $\hat{S}_\alpha$  and  $\hat{V} = |\psi_0\rangle \langle \psi_0|$  is the projector on the initial state  $|\psi_0\rangle$ . In this work, we use Bloch coherent states as the initial states, and choose the generator whose expectation value  $\langle \hat{S}_\alpha \rangle$  is maximised under the initial state. Furthermore, we work with sufficiently small  $\delta \ll 1$ , such that the FOTOC simplifies to the variance of the generator  $\hat{S}_\alpha$ , as  $C(t) \approx \delta^2 \text{var}[\hat{S}_\alpha(t)] + O(\delta^3)$  [10, 28]. The predicted value of the FOTOC for the infinite temperature ‘uniform diagonal ensemble’ (UDE) is  $C_{\text{UDE}} = \delta^2 N(N+2)/12$  [16].

Figure 1(a) shows the dynamics of the FOTOC in the saddle-point and chaotic regimes. In contrast to the behaviour near a stable fixed point, where the FOTOC remains small and bounded, here the FOTOCs grow exponentially until they approach the respective values predicted by the ETH. However there is a marked difference in the long-time behaviours between two regimes. The saddle point FOTOCs exhibit considerable variability around the diagonal-ensemble predictions. This variability is especially marked for an initial state centred directly on the saddle point, where it is manifest in large oscillations. These oscillations occurred for all system sizes we simulated ( $N = 10^1$ ,  $N = 10^2$ ,  $N = 10^3$ ) and are comparable to the maximum values of the FOTOC. As we discuss further below, these oscillations are associated with (near) revivals of the initial state. In contrast, in the chaotic regime the FOTOC does not exhibit regular oscillations but saturates to the uniform diagonal ensemble prediction with only small-amplitude fluctuations for sufficiently large  $N$ , as predicted by the eigenstate thermalisation hypothesis [18].

The differences between the chaotic and saddle point

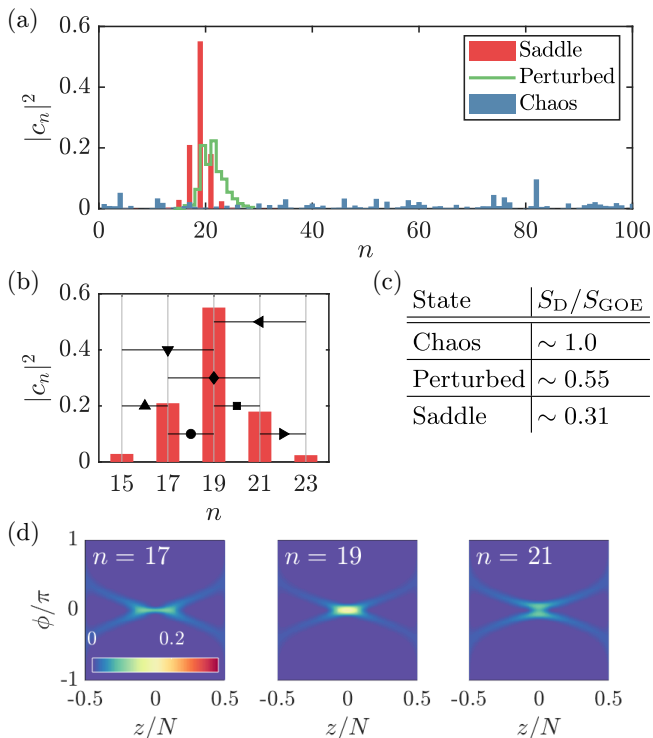


FIG. 2. a) Diagonal distributions of coherent states in chaotic phase space (blue bars), on a saddle point (red bars) and slightly perturbed from the saddle point (green staircase), as in Fig. 1. The distributions are ordered by energy/quasienergy magnitude and indexed by  $n$ . b) Close-up of saddle point diagonal distribution with selected high-overlap energy eigenstate transitions labelled by black markers, corresponding to frequencies identified in Fig. 3(a-b). c) Diagonal entropies of representative states relative to the Gaussian orthogonal ensemble (GOE) prediction. d) Saddle point eigenstate  $Q$  distributions for  $N = 100$ , labelled by  $n$ . The three representative eigenstates were selected as the largest overlap with the saddle point coherent state. Parameters are as in Fig. 1.

regimes is even more marked in the dynamics of the entanglement entropy. In this paper, we calculate von Neumann entropy of the reduced density matrix  $\hat{\rho}_s$  obtained after tracing out  $N - s$  particles [29]:  $\mathcal{S}_E(\hat{\rho}_s) = -\text{Tr}[\hat{\rho}_s \ln(\hat{\rho}_s)]$ . Figure 1(b) shows the half-system ( $s = N/2$ ) entanglement entropy as a function of time. In the chaotic regime, the entanglement entropy grows almost monotonically, and shows very little variation once it saturates at the Page curve prediction. In contrast, the saddle point entanglement entropy exhibits markedly periodic oscillations with distinct revivals. The size of the oscillations means that the system periodically almost completely disentangles. These disentangling points coincide with time at which  $C(t) \approx 0$ , illustrating the close connection between the dynamics of entanglement entropy and FOTOCs previously observed in Ref. [10].

The lack of fluctuations in the entanglement entropy after the Ehrenfest time means that its long-time value is

very well defined, which allows us to test its scaling with system size. To obtain the results in Fig. 1(c), we time-average the entropy after saturation, over the period  $20 \leq J_0 t \leq 200$ . The vertical lines indicate the uncertainty. For small subsystems, the chaotic post-Ehrenfest entanglement entropy matches that of the infinite-temperature uniform diagonal ensemble, but diverges for larger subsystems. The volume law scaling of the chaotic state entanglement entropy matches the Page curve, the average entanglement entropy of a subsystem given the whole system is in a random pure state [30]. For a bipartite system with subsystems  $A, B$  of Hilbert space dimensions  $d_{A,B}$  satisfying  $d_A < d_B$ , this quantity is

$$\langle \mathcal{S}_E(\hat{\rho}_A) \rangle = \Psi(d_A d_B + 1) - \Psi(d_B + 1) - \frac{d_A - 1}{2d_B}, \quad (3)$$

where  $\Psi(x) = \Gamma'(x)/\Gamma(x)$  is the digamma function. In the Dicke state subensemble representation we use [29],  $d_A = s + 1$  and  $d_B = N + 1$ , where  $0 \leq s \leq N$ .

The qualitative differences in the long-time dynamics of the two regimes can be traced back to the eigenstructure, which we probe through the diagonal entropy [17], defined as the von Neumann entropy of the diagonal ensemble,

$$\mathcal{S}_D(\psi) = \sum_n |\langle \psi | \Phi_n \rangle|^2 \ln \left( |\langle \psi | \Phi_n \rangle|^2 \right), \quad (4)$$

with initial coherent state  $|\psi\rangle$  and eigenstates  $|\Phi_n\rangle$ . The diagonal entropy quantifies the delocalisation of the state  $|\psi\rangle$  in the basis of energy eigenstates, or Floquet modes in the case of a Floquet system. According to the eigenstate thermalisation hypothesis (ETH), sufficiently delocalised states are expected to thermalise [18]. The Gaussian orthogonal ensemble (GOE) of random matrices gives a prediction of  $\mathcal{S}_{GOE} \approx \ln[0.48(N + 1)]$  [17] for fully thermalising states under the Bose-Hubbard Hamiltonian (1), which is real and symmetric.

The diagonal distributions of the states used in the chaotic and saddle-point regimes are shown in Fig. 2(a), with the corresponding diagonal entropies in Fig. 2(c). The chaotic state matches the GOE prediction, indicating that a large number of eigenstates participate in the FOTOC dynamics and the state will thermalise. In contrast, the diagonal entropy of the saddle point state is much smaller than the GOE prediction, indicating that relatively few eigenstates participate in the FOTOC dynamics and the state will not thermalise. The three dominant eigenstates are illustrated in Fig. 2(d) and are all highly localised around the saddle point. The saddle-perturbed state has intermediate diagonal entropy and thus exhibits small amplitude FOTOC oscillations without distinct revivals or saturation. The diagonal distribution of a state centred on a stable fixed point is almost a delta distribution ( $\mathcal{S}_D \approx 0$ ) and therefore the state's FOTOC and entanglement entropy are predicted to be nearly time-independent, which matches our observations.

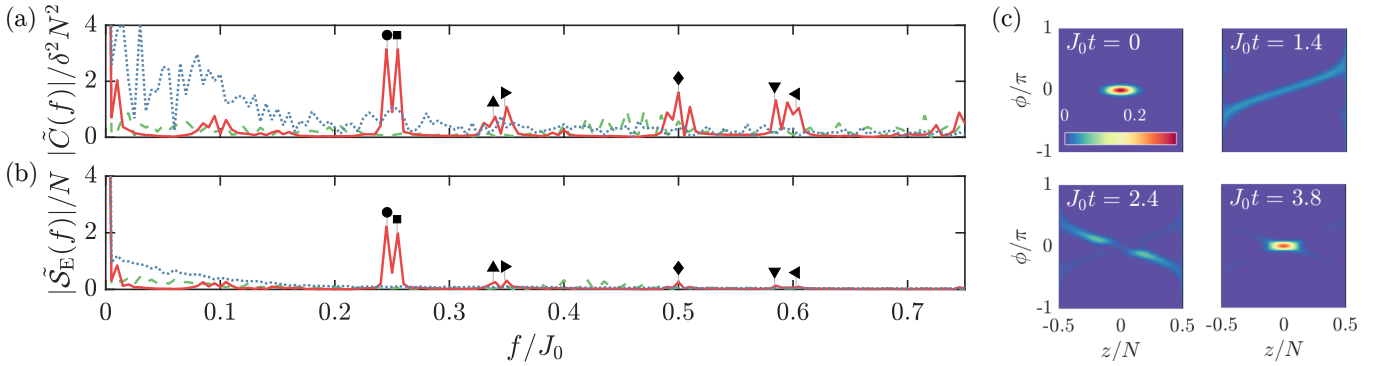


FIG. 3. a) Fourier spectra of fidelity out-of-time-order correlators (FOTOCs) for chaotic phase space (blue dotted line), a saddle point (red line) and a point slightly perturbed from the saddle point (green dashed line) for  $N = 100$  particles. b) Fourier spectra of von Neumann entanglement entropy for a subsystem of  $s = N/2$  Dicke states and  $N = 100$  particles. In both plots, high-occupancy energy eigenstate transition frequencies for the saddle point state are indicated by black markers, corresponding to Fig. 2(b). Parameters are as in Fig. 1. c) Saddle point state  $Q$  distribution dynamics for  $N = 100$ .

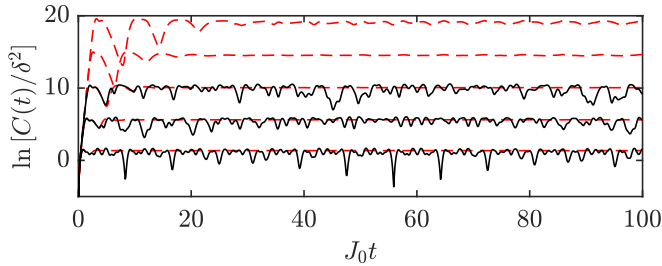


FIG. 4. Fidelity out-of-time-order correlators (FOTOCs) for the saddle point in Fig. 1 for  $N = 10^p$  particles, where  $p = 1, 2, 3, 4, 5$  from the bottom. Exact dynamics are indicated by black solid lines and truncated Wigner approximations are indicated by red dashed lines. Exponential short-time FOTOC growth is evident and the Ehrenfest (scrambling) time increases with  $N$ .

The connection between the diagonal ensemble and the FOTOC and entanglement dynamics is clearly revealed in the Fourier spectra of these quantities. As evident in Fig. 3(a), the saddle-point FOTOC spectrum displays distinct peaks at frequencies corresponding to the transition energies between eigenstates that dominate the diagonal ensemble. These eigenstates can be identified by their distinctly high overlaps with the evolving state, shown in Fig. 2(b).

The Fourier spectrum of the entanglement entropy displays much of the same features as that of the FOTOC for  $N = 100$ . The Fourier spectrum of the saddle-point entropy has few, sharp peaks, while those of the chaotic phase space and saddle-perturbed state exhibit no distinct peaks. The appearance of beating in the saddle-point entanglement entropy dynamics is evident in the double-peaked Fourier spectrum, giving oscillation period  $T_o \approx 4.00/J_0$  and beat period  $T_b \approx 106/J_0$ . The beat period can be interpreted as the partial revival timescale. Periodic partial revivals are similarly evident in the long-time dynamics of the  $N = 1000$  saddle point

FOTOC in Fig. 1(a).

That so few eigenstates participate in the saddle-dominated dynamics is the reason why these regular revivals are so substantial. The revival dynamics is illustrated qualitatively in the phase-space  $Q$  distribution, shown in Fig. 3(d). The coherent state, initially located on the saddle point, is periodically sheared along the separatrix and extends around the Bloch sphere before the separate  $Q$  distribution arms recombine at the saddle point, leading to a fairly complete reconstruction of the initial coherent state. This periodic dividing and recombining is the source of the oscillatory FOTOC behaviour.

Finally, we use our exact calculations to benchmark the truncated Wigner method, an approximate approach that can allow simulation of larger Hilbert spaces. As shown in Fig. 4, the Wigner method correctly predicts the rapid exponential growth of the FOTOC up until the Ehrenfest time. However, it completely fails to reproduce the persistent fluctuations seen in the long term dynamics, which signal the lack of thermalisation in the saddle point regime. This failure of the Wigner simulations in the case of the Bose-Hubbard dimer is in contrast with the unstable fixed-point dynamics observed for the Dicke model [15], where fluctuations after the Ehrenfest time are absent.

#### IV. CONCLUSIONS

We studied the long-time dynamics of the fidelity out-of-time-order correlator and entanglement entropy for a system of ultracold atoms in the presence of chaos and in the vicinity of a saddle point in integrable phase space, finding that a state located on the saddle point fails to thermalise. The Bose-Hubbard dimer saddle point FOTOC and entanglement entropy dynamics were distinctly periodic, with dominant frequencies given by transition energies between eigenstates with high overlap on the evolving state. Perturbing a state slightly from the sad-

dle point resulted in aperiodic FOTOC and entanglement entropy dynamics that nevertheless failed to thermalise completely, exhibiting persistent oscillations. The diagonal entropy of the initial state correctly predicted the degree of thermalisation regardless of short-time FOTOC behaviour, suggesting that this aspect of chaos is independent of saddle point scrambling.

In order to distinguish clearly the different characteristics of the chaos-induced thermalisation versus saddle-

point-driven scrambling, we have chosen regimes where there is either a saddle point or chaos in the semiclassical phase space, but not both. For regimes where both are present, the OTOC growth may reflect an interplay of the two, such that the long-term thermal behaviour arises from the chaotic nature of the system, but where the initial rapid growth in correlations—and hence Lyapunov exponent—is determined by the saddle point.

- 
- [1] P. Hayden and J. Preskill, *J. High Energy Phys.* **2007** (09), 120.
  - [2] Y. Sekino and L. Susskind, *J. High Energy Phys.* **2008**, 065 (2008).
  - [3] S. H. Shenker and D. Stanford, *J. High Energy Phys.* **2014** (12), 46.
  - [4] D. A. Roberts, D. Stanford, and L. Susskind, *J. High Energy Phys.* **2015** (3), 51.
  - [5] P. Hosur, X.-L. Qi, D. A. Roberts, and B. Yoshida, *J. High Energy Phys.* **2016** (2), 4.
  - [6] J. Maldacena, S. H. Shenker, and D. Stanford, *J. High Energy Phys.* **2016** (8), 106.
  - [7] E. B. Rozenbaum, S. Ganeshan, and V. Galitski, *Phys. Rev. Lett.* **118**, 086801 (2017).
  - [8] J. Rammensee, J. D. Urbina, and K. Richter, *Phys. Rev. Lett.* **121**, 124101 (2018).
  - [9] I. García-Mata, M. Saraceno, R. A. Jalabert, A. J. Roncaglia, and D. A. Wisniacki, *Phys. Rev. Lett.* **121**, 210601 (2018).
  - [10] R. J. Lewis-Swan, A. Safavi-Naini, A. M. Kaufman, and A. M. Rey, *Nat. Rev. Phys.* **1**, 627 (2019).
  - [11] R. Prakash and A. Lakshminarayan, *Phys. Rev. B* **101**, 121108(R) (2020).
  - [12] T. Xu, T. Scaffidi, and X. Cao, *Phys. Rev. Lett.* **124**, 140602 (2020).
  - [13] M. Gärttner, J. G. Bohnet, A. Safavi-Naini, M. L. Wall, J. J. Bollinger, and A. M. Rey, *Nat. Phys.* **13**, 781 (2017).
  - [14] M. Gärttner, P. Hauke, and A. M. Rey, *Phys. Rev. Lett.* **120**, 040402 (2018).
  - [15] S. Pilatowsky-Cameo, J. Chávez-Carlos, M. A. Bastarrachea-Magnani, P. Stránský, S. Lerma-Hernández, L. F. Santos, and J. G. Hirsch, *Phys. Rev. E* **101**, 010202(R) (2020).
  - [16] R. A. Kidd, A. Safavi-Naini, and J. F. Corney, *Phys. Rev. A* **102**, 023330 (2020).
  - [17] L. D'Alessio, Y. Kafri, A. Polkovnikov, and M. Rigol, *Adv. Phys.* **65**, 239 (2016).
  - [18] M. Rigol, V. Dunjko, and M. Olshanii, *Nature* **452**, 854 (2008).
  - [19] S. Pappalardi, A. Russomanno, B. Žunkovič, F. Iemini, A. Silva, and R. Fazio, *Phys. Rev. B* **98**, 134303 (2018).
  - [20] Q. Hummel, B. Geiger, J. D. Urbina, and K. Richter, *Phys. Rev. Lett.* **123**, 160401 (2019).
  - [21] A. Bhattacharyya, W. Chemissany, S. S. Haque, and B. Yan, *arXiv:1909.01894 [hep-th]* (2019).
  - [22] T. Ali, A. Bhattacharyya, S. S. Haque, E. H. Kim, N. Moynihan, and J. Murugan, *Phys. Rev. D* **101**, 026021 (2020).
  - [23] K. Hashimoto, K.-B. Huh, K.-Y. Kim, and R. Watanabe, *arXiv:2007.04746 [hep-th]* (2020).
  - [24] A. Bhattacharyya, W. Chemissany, S. S. Haque, J. Murugan, and B. Yan, *arXiv:2007.01232 [hep-th]* (2020).
  - [25] G. J. Milburn, J. Corney, E. M. Wright, and D. F. Walls, *Phys. Rev. A* **55**, 4318 (1997).
  - [26] G. J. Milburn, J. F. Corney, D. Harris, E. M. Wright, and D. F. Walls, in *Photonics West '97: Atom Optics*, SPIE Proceedings, Vol. 2995, edited by M. G. Prentiss and W. D. Phillips (SPIE, Bellingham, WA, 1997) pp. 232–239.
  - [27] R. A. Kidd, M. K. Olsen, and J. F. Corney, *Phys. Rev. A* **100**, 013625 (2019).
  - [28] M. Schmitt, D. Sels, S. Kehrein, and A. Polkovnikov, *Phys. Rev. B* **99**, 134301 (2019).
  - [29] F. Fröwis, R. Schmied, and N. Gisin, *Phys. Rev. A* **92**, 012102 (2015).
  - [30] E. Bianchi and P. Donà, *Phys. Rev. D* **100**, 105010 (2019).